Meteorol. Appl. 6, 371–383 (1999)

Observations and model simulations of a winter sub-synoptic vortex over the central Mediterranean

K Lagouvardos, V Kotroni, S Nickovic, D Jovic, G Kallos, *University of Athens, Meteorology Laboratory, Athens, Greece*

C J Tremback, *Mission Research Corporation/*ASTER Division, Fort Collins, USA*

A sub-synoptic vortex with characteristics of a tropical storm developed over the area between Italy and Greece, during the period 14–18 January 1995. Satellite imagery revealed that this vortex was associated with spirally distributed bands and a clearly defined 'eye'. Ship reports and SSM/I retrieved winds show the existence of strong surface winds around the vortex. Simulation of the genesis and life-cycle of the vortex using the Regional Atmospheric Modelling System and the Eta model successfully reproduced the vortex formation, its strength and its path towards the northern African coast. The model results showed the importance of the surface fluxes (sensible and latent heat) in the development of the vortex on the rear side of a parent low-pressure system which was advected towards the east. During the mature stage of the vortex, latent-heat release within the convective motions was the dominant mechanism which sustained the vortex until its landfall.

1. Introduction

From 14 to 18 January 1995 a convective perturbation with features similar to a mature tropical storm was depicted in satellite imagery over the central Mediterranean, between Italy and Greece. This 'tropical storm', which can be distinguished as a sub-synoptic vortex-like disturbance, presented several interesting characteristics:

- a clearly defined 'eye', reminiscent of a tropical cyclone, and spirally distributed cloudbands around the 'eye';
- a warm core;
- a band of strong winds at lower levels close to the vortex centre;
- small dimension (~150 km radius);
- rather long life-time (~3 days).

Such phenomena do not occur very often in the Mediterranean region. Over the 15 years from 1982 to 1996 four similar cases were reported over the Mediterranean Sea: on 26–28 January 1982, 26 March 1983, 27 September – 1 October 1983, and 29–30 December 1984 (Ziakopoulos & Marinaki, 1996). So far the best documented cases of this kind are the storm of 26 January 1982 (Mayencon, 1982; Ernst & Matson, 1983; Businger & Reed, 1989) and the sub-synoptic vortex of 27 September 1983 (Rasmussen & Zick, 1987). Ziakopoulos & Marinaki (1996) reported that all these cases had the characteristics of tropical storms, with a clearly defined 'eye', spirally distributed cloud bands, and strong winds. Alpert & Neeman (1992) studied cold small-scale cyclones in the Mediterranean area and suggested that some of them presented polar low-like features which were not resolvable in their analysis due to the lack of high-resolution data. The vortex studied in this paper has also prompted the work by Santurette (1995), who presented a brief description of the meteorology and a series of satellite pictures of this event.

Following the classification of Businger & Reed (1989), these Mediterranean disturbances can be described as 'cold-low-type' polar lows, which occur when cold air masses are advected over a warmer sea. The authors distinguished three elementary types of polar low development based on their distinct synoptic pattern and classified the aforementioned disturbances over the Mediterranean Sea as 'cold-low type' polar lows, which are characterised by strong surface fluxes and deep convection. In the light of this classification, the 14–18 January 1995 vortex will be analysed with the aim of investigating whether this vortex has 'cold-low-type' features.

The vortex described in this paper formed behind a pre-existing low centre, which progressed from the maritime area west of Greece towards the east, while the vortex independently moved southwards during the next three days. As mentioned by Ziakopoulos & Marinaki (1996), the operational model (T213/L31) of the European Centre for Medium-Range Weather Forecasts (ECMWF) predicted the translation of the

low centre and the associated front towards the east. However, the forecast of the vortex formation failed, showing only a weak cyclonic circulation over the area where the vortex was observed. Businger & Reed (1989) underlined that in cases where the lows grow spontaneously from infinitesimal disturbances the systems are inherently unpredictable, mainly in the incipient stage, by operational forecast systems. These authors argued that the scale of these disturbances is too small for numerical weather prediction models to provide adequate forecast guidance. The limited usefulness of the operational models to predict polar lows (including Mediterranean vortices) and the problem of making the actual forecast prompted this study.

The objectives of this research are the following:

- to document the appearance of this Mediterranean vortex and compare it with earlier observations of polar lows as well as with the few earlier observational studies of vortices in the Mediterranean.
- to investigate the ability of two atmospheric models, regularly used for regional weather forecasting and research, to accurately predict the genesis and life-cycle of this vortex.
- to explore the underlying physical mechanisms associated with the formation and life-cycle of this vortex using model results.

This investigation will be based on many of the available observations in the region (mainly satellite imagery and ship reports) as well as on the use of two numerical models. The models used in this study are:

- a version of the Eta model which is called SKIRON. The SKIRON model is used for operational regional forecasts at the Hellenic National Meteorological Service.
- the Regional Atmospheric Modeling System (RAMS), which was developed as a research model, and is starting to be used extensively as an operational model (e.g., Cotton *et al.*, 1994; Tremback *et al.*, 1994).

This paper is organised as follows. In section 2, the observational evidence of the vortex is given. Section 3 describes the models used for this study as well as the specific set-ups used for the simulations. Section 4 is devoted to a discussion of the model results. In the last section, possible mechanisms responsible for the generation, development and life-cycle of the vortex are discussed.

2. Observational evidence

On 13 January 1995 a 1040 hPa anticyclone was offshore of France moving progressively over Western Europe while at 500 hPa a trough with an axis oriented north-east–south-west was located over the Balkans, Italy and central Mediterranean (not shown). From 1200 UTC on 12 January to 1200 UTC on 13 January, a cooling of about 10 K at 500 hPa, 8 K at 700 hPa and 3 K at 850 hPa occurred over the central Mediterranean, as reported by sounding measurements at Sicily and Malta (for the locations see Figure 5). At 1200 UTC on 14 January (Figure 1(*a*)), the anticyclone moved over Central Europe, while a surface cold front is evident in the area south of Greece, associated with a 992 hPa low-pressure system (called the parent low, hereafter) while an occluding process has started over the sea west of Greece. From that time on, the feed of cold air is interrupted. Twenty-four hours later (1200 UTC, 15 January), a secondary low is created in the region of the decaying occlusion (Figure 1(*b*)), while the parent low moves farther towards the east. From

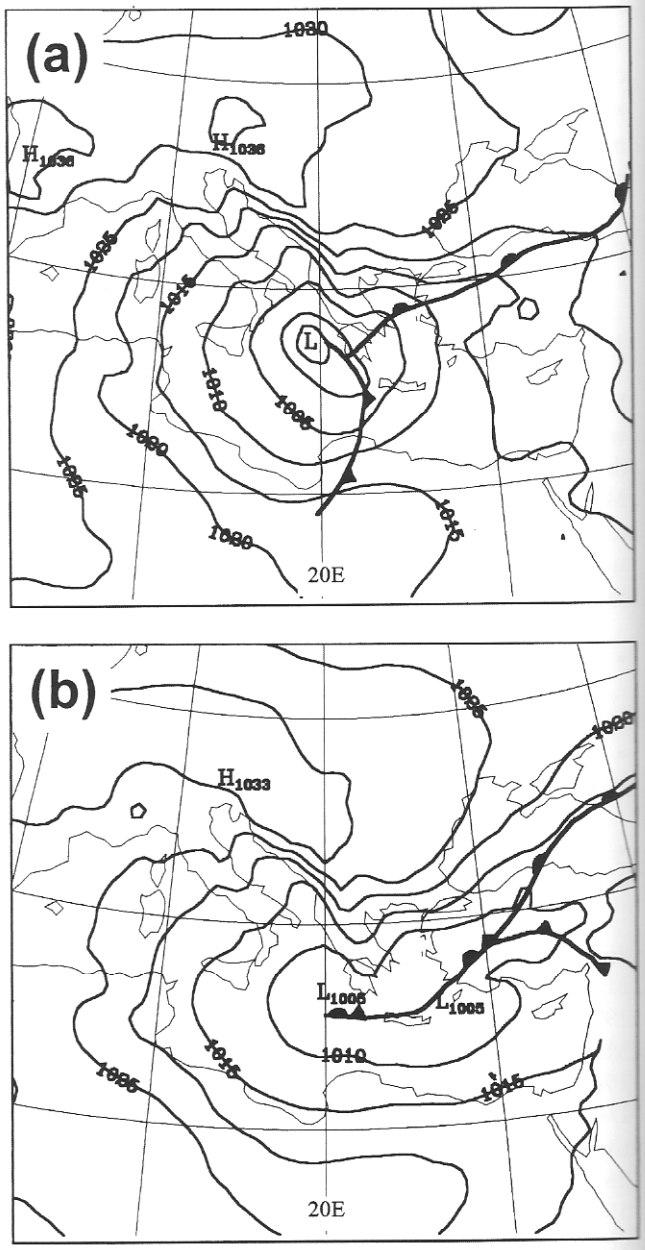

Figure 1. *Surface map at* (a) *1200 UTC on 14 January 1995 and* (b) *at 1200 UTC on 15 January (isobars plotted every 5 hPa).*

that time, the secondary low becomes independent of the parent low and during the next three days it follows a path towards the south, approximately parallel to the 20° E meridian. The storm dissipates during 18 January 1995, when it reaches the northern African coasts.

From satellite imagery a detailed insight into the characteristics of the storm may be gained. Figure 2(*a*) shows the position of the storm at 1200 UTC on 14 January and the 500 hPa chart. The cloud structure associated with the parent low is evident while a cut-off low is also observed at the 500 hPa level over Sicily. As pointed out by Businger (1985), the existence of large cold pools of cyclonically rotating air provide the most favourable environment for polar low development over the Arctic Ocean. The Brindisi sounding (Brindisi is denoted by the letter B in Figure 2(*a*)) at the same time revealed that near saturated conditions prevail from 925 up to the 500 hPa level (not shown). A superadiabatic lapse rate is evident in the lowest layers up to 900 hPa, while the lower tropospheric layers are characterised by a strong north-eastern flow from the Balkans towards the Mediterranean Sea.

At 1200 UTC on 15 January, the cloud structure of the disturbance shows characteristics of a tropical storm with spirally distributed cloud bands around a cloud-free circular area, the 'eye' of the storm. A cut-off low is situated over the storm (Figure 2(*b*)). As the storm moved southwards it became very distant from any upper-air station, and thus there was no information about the vertical stability in the vicinity of the storm.

By 0000 UTC on 16 January, the storm has progressed 100 km southwards following a path almost parallel to the 20° E meridian (not shown). Six hours later, the storm reaches its mature stage (Figure 2(*c*)). Deep convective clouds are spirally distributed at a radius of ~150 km around the 'eye', while lower clouds with a spiral structure (mainly on the northern side of the vortex) are evident at a radius of ~200 km around the vortex center. Note also the presence of low clouds over the Aegean Sea and the blocking effect of the Cretan mountains on the progress of the clouds towards the south.

The synoptic observations over the central and eastern Mediterranean as well as reports from ships allow the analysis of the wind and temperature field associated with the storm. Moreover these observations will provide a basis for comparison with the predictions from the numerical models. In the early stages of development of the disturbance (1200 UTC, 14 January), two ships travelling between Italy and Greece reported winds of 22 m s^{-1} and 29 m s^{-1} (denoted respectively by the letters A and B in Figure 3(*a*)). Ship A reported a 992.5 hPa pressure near the centre of the parent low. Twenty-four hours later, two low centres are observed (Figure 3(*b*)), one over the Aegean Sea associated with the parent low, which has moved eastwards, and a

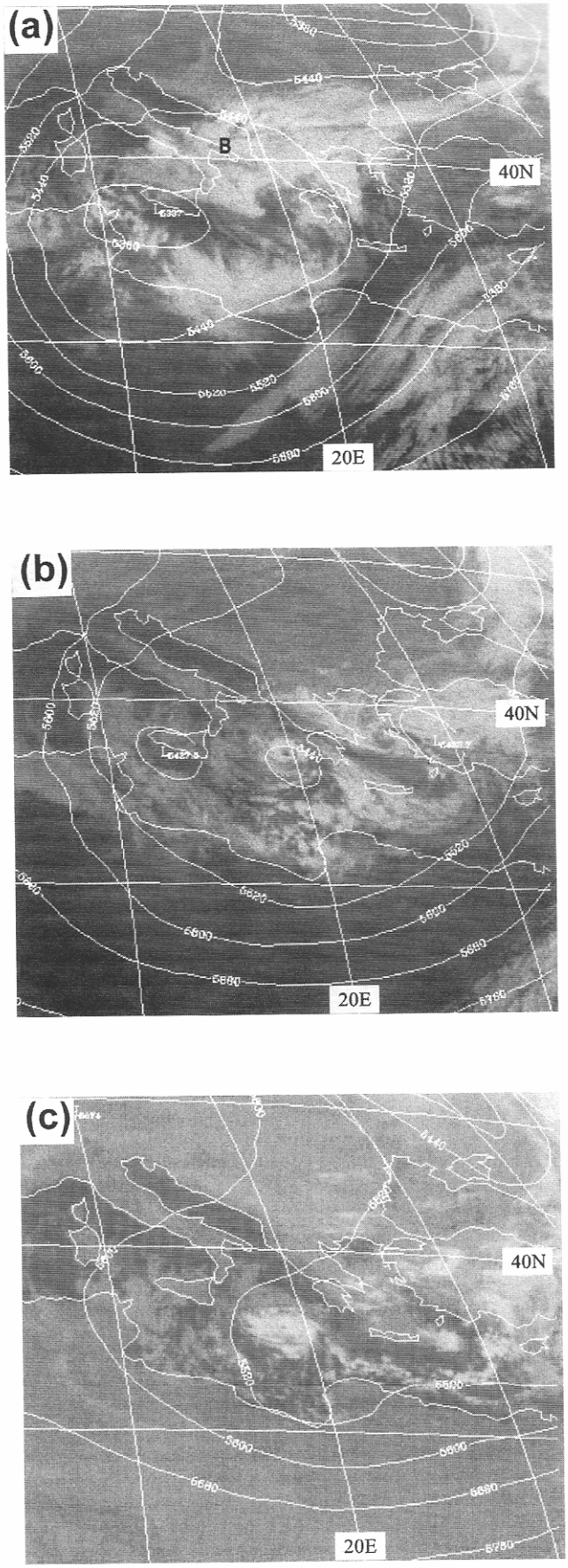

Figure 2. *METEOSAT infrared satellite images of the vortex and 500 hPa geopotential height (contours plotted every 80 m) at* (a) *1200 UTC on 14 January 1995,* (b) *1200 UTC on 15 January, and* (c) *0600 UTC on 16 January, 1995.*

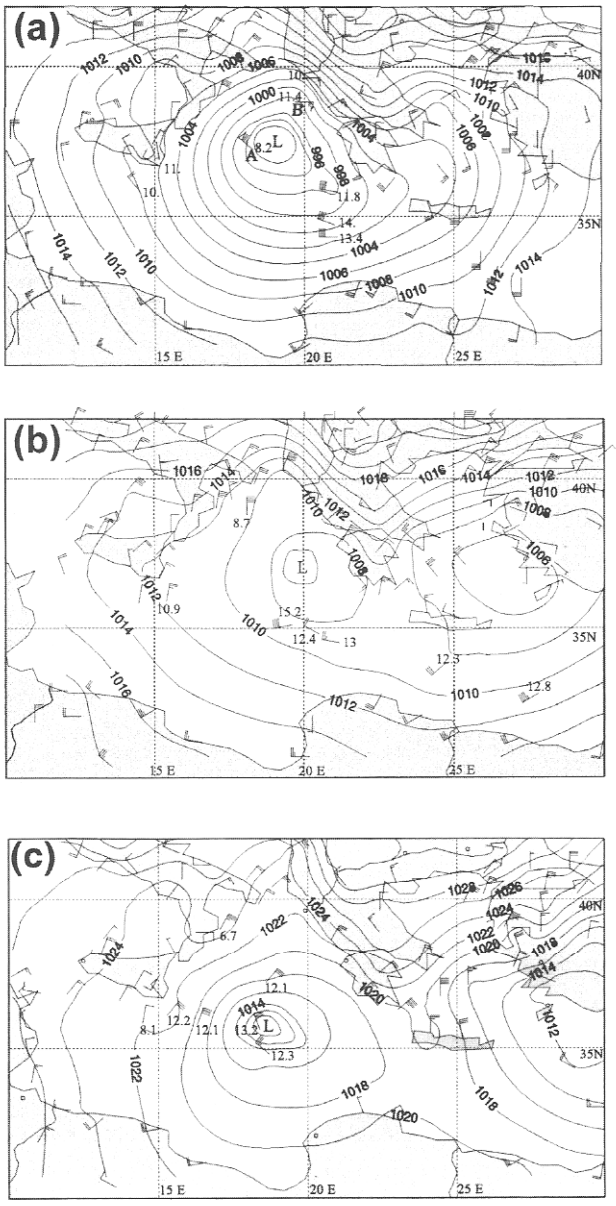

Figure 3. *Surface pressure subjective analysis (isobars plotted every 2 hPa) at* (a) *1200 UTC on 14 January,* (b) *1200 UTC on 15 January, and* (c) *0600 UTC on 16 January 1995. One pennant equals 20 m s^{-1}, one barb 4 m s^{-1} and one half-barb 2 m s^{-1}. A few temperature reports from ships (in °C) are also plotted. The letters* A *and* B *in* (a) *are referred to in the text.*

second in the maritimc arca west of Peloponnissos associated with the sub-synoptic vortex (see also the satellite image, Figure 2(*b*)). At 0600 UTC on 16 January four ships provided reports from the vicinity of the disturbance (Figure 3(*c*)). The ship nearest to the vortex centre (35.7° N, 18.2° E) reported a 23 m s^{-1} surface wind and a pressure of 1009 hPa. The wind speed indicates that at this time the system has reached tropical storm intensity. The same ship also reported a 13.2 °C air temperature, which is the highest temperature within the whole domain shown in Figure 3(*c*), suggesting that the vortex possesses a warm core. This inference is consistent with earlier observations of polar lows (e.g. Rasmussen, 1981; Businger & Baik, 1991; Douglas *et al.*, 1991) and of Mediterranean vortices (Rasmussen & Zick, 1987). At 1200 UTC on 16 January only one ship reported data near the vortex centre with a 25 m s^{-1} easterly wind and 13 °C air temperature, which is again among the highest temperatures reported in the central and eastern Mediterranean at that time (not shown).

Although the route of some ships covered the area of the vortex, the information about the wind field pattern is still incomplete. In order to gain a better insight of the wind field, data provided by the Special Sensor Microwave/Imager (SSM/I) on board the Defence Meteorological Satellite Program (DMSP) space vehicles can be used. For that reason, radiances from the five channels of the SSM/I have been combined following the formula proposed by Schluessel & Luthardt (1991). The wind field corresponding to the passage of the satellite at 1607 UTC on 16 January is presented in Figure 4. This shows strong winds in the vicinity of the storm with a maximum of 28 m s^{-1} near the northern flank of the system. Strong marine winds are also found over the Aegean Sea, corresponding to the northerly winds associated with the parent low which at that time is located near the Turkish coasts.

3. Model description and set-up

3.1. The Eta model

The Eta model was developed at the University of Belgrade (dynamical part) and the National Centers for Environmental Prediction at Washington (physical parameterisations). Details about the Eta model can be found in Janjic (1984, 1990, 1994) and Mesinger *et al.* (1988). The model uses the semi-staggered E grid in the horizontal and the eta coordinate (a generalised sigma coordinate with step-like mountains) in the vertical.

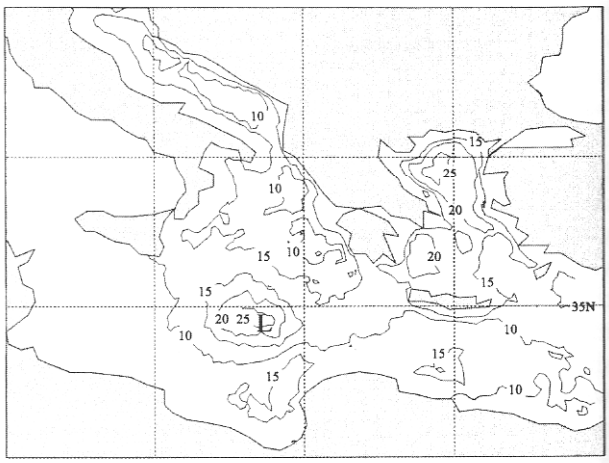

Figure 4. *Maritime wind speed (isotachs plotted every 5 m s^{-1}) estimated from SSM/I data, at 1607 UTC on 16 January 1995. The letter* L *denotes the low centre.*

The model was initialised at 0000 UTC on 14 January 1995 and ran over 84 hours. In the horizontal, a 0.2° grid interval has been used. The model top was set at the 100 hPa level. Thirty-two vertical levels were used, with the lowest model level placed 60 m above the model topography or sea, having approximately 90 m vertical spacing at the lower level over the sea and 135 m over topography, stretching to 1.1 km at the top of the domain. In the lower atmosphere, model levels either coincide with tops of the mountain grid boxes, or intersect the mountain elements. In addition, the Eta model includes:

- a non-radiation condition at the model top boundary;
- a lateral boundary condition based on a simple averaging method;
- no-slip bottom boundary conditions at the mountain boxes;
- the Betts–Miller convection scheme revised by Janjic (1990, 1994), a simple large-scale precipitation scheme;
- a turbulent mixing scheme (Janjic, 1994) based on the Mellor–Yamada model.

A similar model set-up is currently used for operational forecasts at the Hellenic National Meteorological Service.

For the present study the domain of integration covered the central and eastern Mediterranean (Figure 5). The model was initialised using analyses provided by the ECMWF with a resolution of 1° × 1°. These fields were also used to update the lateral boundary conditions every six hours. The model was executed using observed sea-surface temperature fields provided by ECMWF with a resolution of 1° × 1° (Figure 5). Finally, the model topography is derived from a 30″ × 30″ resolution terrain data set.

3.2. The RAMS model

The Regional Atmospheric Modeling System (RAMS) was developed at Colorado State University. A general description of the model and its capabilities is given in Pielke *et al.* (1992). For the present application, RAMS was initialised at 0000 UTC on 14 January 1995 and the duration of the simulation was 72 hours. The non-hydrostatic version of the model is employed, using three nested grids:

- Grid 1. The outer grid, with a mesh of 71 × 48 points and a 60 km horizontal grid interval.
- Grid 2. The intermediate grid with 94 × 86 points and a 15 km horizontal grid interval.
- Grid 3. The inner grid with 122 × 140 points and a 5 km horizontal grid interval.

The location and horizontal extension of each grid are presented in Figure 5. Grid 3 was used for an 18-hour

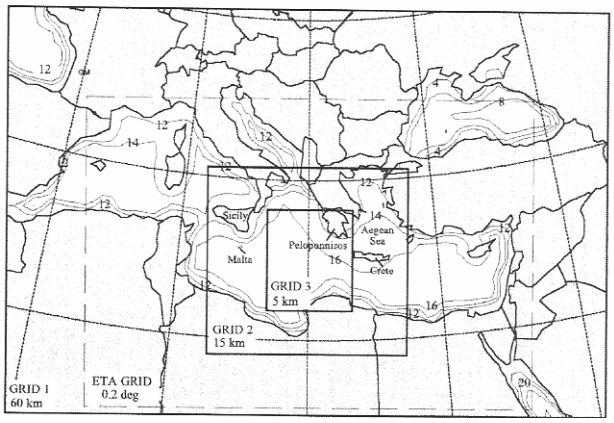

Figure 5. *Horizontal extension of the Eta grid (dashed rectangle) and three nested grids of RAMS (Grid 1, Grid 2 and Grid 3). For each grid the horizontal grid length is also given. Sea-surface temperature field used by both models is also reported at 2 °C interval.*

period starting at 1800 UTC on 15 January because of the higher CPU-cost of the three-grid simulation.

Twenty-five levels following the topography were used for all grids. The vertical spacing varied from 120 m near the surface to 1 km at the top of the model domain (z = 15.5 km). Along with these settings, other RAMS configuration options included:

- A rigid lid was set at the model top boundary.
- The lateral boundary conditions on the outer grid used a the relaxation scheme similar to that of Davies (1976).
- The full microphysical package of RAMS was activated. This package includes the condensation of water vapour to cloud water when supersaturation occurs as well as the prognosis of rain, graupel, pristine ice, aggregates, and snow species.
- A Kuo-type cumulus parameterisation scheme developed by Tremback (1990) was used because the model-resolved convergence produced at the scales of Grid 1 (60 km) and Grid 2 (15 km) is not enough to explicitly initiate convection. For Grid 3 (5 km), the cumulus parameterisation scheme was not activated because of the assumptions implicit in this scheme (Cram *et al.*, 1992).

The ECMWF 1° × 1° gridded analysis fields were used in order to initialise the model. The ECMWF data are objectively analysed by the RAMS model on isentropic surfaces from which they are interpolated to the RAMS grids. These fields were used in order to nudge the lateral boundary region of Grid 1 every six hours. Because of the importance of sea to air fluxes in the formation and maintenance of this storm, observed sea-surface temperature data of 1° × 1° resolution provided by ECMWF have been used (Figure 5). Moreover, topography derived from a 30″ × 30″ terrain data and gridded vegetation-type data of 10′ × 10′ resolution have been

used. In order to investigate the role of latent heat release in the convective motions on the vortex life-cycle, an additional simulation has been performed where the microphysics package was not activated.

4. Results from the Eta model

The evolution of the sea-level pressure and wind field at the lowest model level (approximately 60 m over the sea) associated with the parent low and the vortex predicted by the Eta model are presented in Figure 6. The 12-hour forecast (1200 UTC, 14 January), has the low centre associated with the parent system located west of Peloponnisos (Greece) with a central pressure of 995 hPa (Figure 6(*a*)). The wind field (Figure 6(*b*)) shows strong northerly winds on the western flank of the low with a maximum of 20 m s^{-1} south of Italy. The model underestimated the strong wind reported by ships on the north-eastern and southern flanks of the system (see Figure 3(*a*), ships denoted by the letters A and B). The south-easterly flow over the Aegean Sea, associated with the warm conveyor belt ahead of the surface cold front, is also predicted by the model. The same applies to the strong north-easterly flow in the northern Aegean Sea, which exceeds 22 m s^{-1}, in good agreement with the observed winds over the north-eastern Aegean Sea (Figure 3(*a*)).

The 36-hour prediction of sea-level pressure in the vortex centre at 1200 UTC on 15 January is 1007 hPa and the centre is now located between Peloponnisos and Sicily, with the strongest gradients on the northern flank of the vortex (Figure 6(*c*)). The strongest winds predicted over the area south of Italy exceed 18 m s^{-1} (Figure 6(*d*)), in good agreement with the 18–20 m s^{-1} wind speeds reported by ships in this area (see Figure 3(*b*)). The predicted wind is much weaker on the southern flank of the vortex, not exceeding 5 m s^{-1}.

In the 54-hour forecast (0600 UTC, 16 January, Figure 6(*e*)), the vortex centre has progressed towards the south, located north of the Libyan coast. The central pressure has increased to 1017 hPa, a value which deviates from a ship report of 1009 hPa (Figure 3(*c*)), and its position is about 150 km to the south, with respect to the observed position of the vortex (Figure 2(*c*)). The wind intensity forecast by the model is about 16 m s^{-1} on the northern and north-western flanks of the vortex (Figure 6(*f*)), a value significantly weaker than that of 23 m s^{-1} reported by a ship at the western flank (Figure 3(*c*)). Six hours later, the central pressure has increased to 1021 hPa, the vortex centre has progressed more to the south, while the wind has slowed to 10 m s^{-1} (not shown). The cyclone was not apparent at the 84-hour forecast (1200 UTC, 18 January), after its landfall on the northern African coast (not shown).

The thermodynamic structure of the vortex during its mature stage within the lower tropopsheric layers can be considered by inspecting the 850 hPa temperature and humidity fields predicted by the model. At 0600 UTC on 16 January the temperature at 850 hPa over the vortex is just above 0 °C, indicating that the vortex possesses a warm core structure (Figure 7(*a*)). This forecast is also in good agreement with the ship reports (Figure 3(*c*)) of a warm core at the surface. The relative humidity field clearly shows good agreement with the observed cloud shield, with near-saturated conditions in the cloudy area, especially on the northern and western flanks of the vortex and lower values (70%) near the centre of the vortex (Figure 7(*b*)). This feature is similar to that provided by aircraft measurements in the vicinity of polar lows (Douglas *et al.*, 1991, 1995).

A better overview of the thermodynamic structure of the vortex can be obtained by inspecting a vertical cross-section inside the vortex core. Figure 8 presents an east–west cross-section (following line *AB* in Figure 7(*a*)) of equivalent potential temperature θ_e valid at 0600 UTC on 16 January 1995. The cross-section shows the existence of the vortex delimited by vertically oriented θ_e contour lines, with a horizontal width of approximately 130–140 km between the 300 K isolines. This structure is evident from sea level up to a height of 3.8 km. Note also that the vortex centre is characterised by a pronounced maximum in θ_e, which exceeds 306 K near the surface. The core of the disturbance is characterised by strong convective instability in the first kilometre, while the atmosphere is also convectively unstable on the periphery of the vortex and up to a height of about 2 km. This characteristic of a pronounced maxima in θ_e at the core of the disturbance was also reported by Businger & Baik (1991) for an Arctic hurricane over the Bering Sea.

5. Results from RAMS

Figure 9 presents the wind field at z = 50 m AGL, predicted using Grid 2 of RAMS (15 km horizontal grid), at two distinct times from the beginning of the simulation. The 12-hour forecast for 1200 UTC on 14 January 1997 (Figure 9(*a*)) has the area of the parent low characterised by strong cyclonic flow, with the strongest wind predicted on the northern and southern flanks of the low centre. Indeed, ship reports (denoted by the letters A and B on Figure 3(*a*) and superimposed on Figure 9(*a*)) are in very good agreement with the RAMS results. Note also the sharp veering of the flow associated with the cold front passage south of Greece. Forty-two hours later at 0600 UTC on 16 January (Figure 9(*b*)) the vortex has moved farther south towards the African coast. The circulation near its centre is weak, while the stronger flow is depicted on the northern and western flanks of the vortex, exceeding 20 ms^{-1}. This wind intensity is consistent with the ship reports of 23 m s^{-1} sustained wind on the western side of the vortex (Figure 3(*c*)). Comparing the model and observational wind patterns, it should be

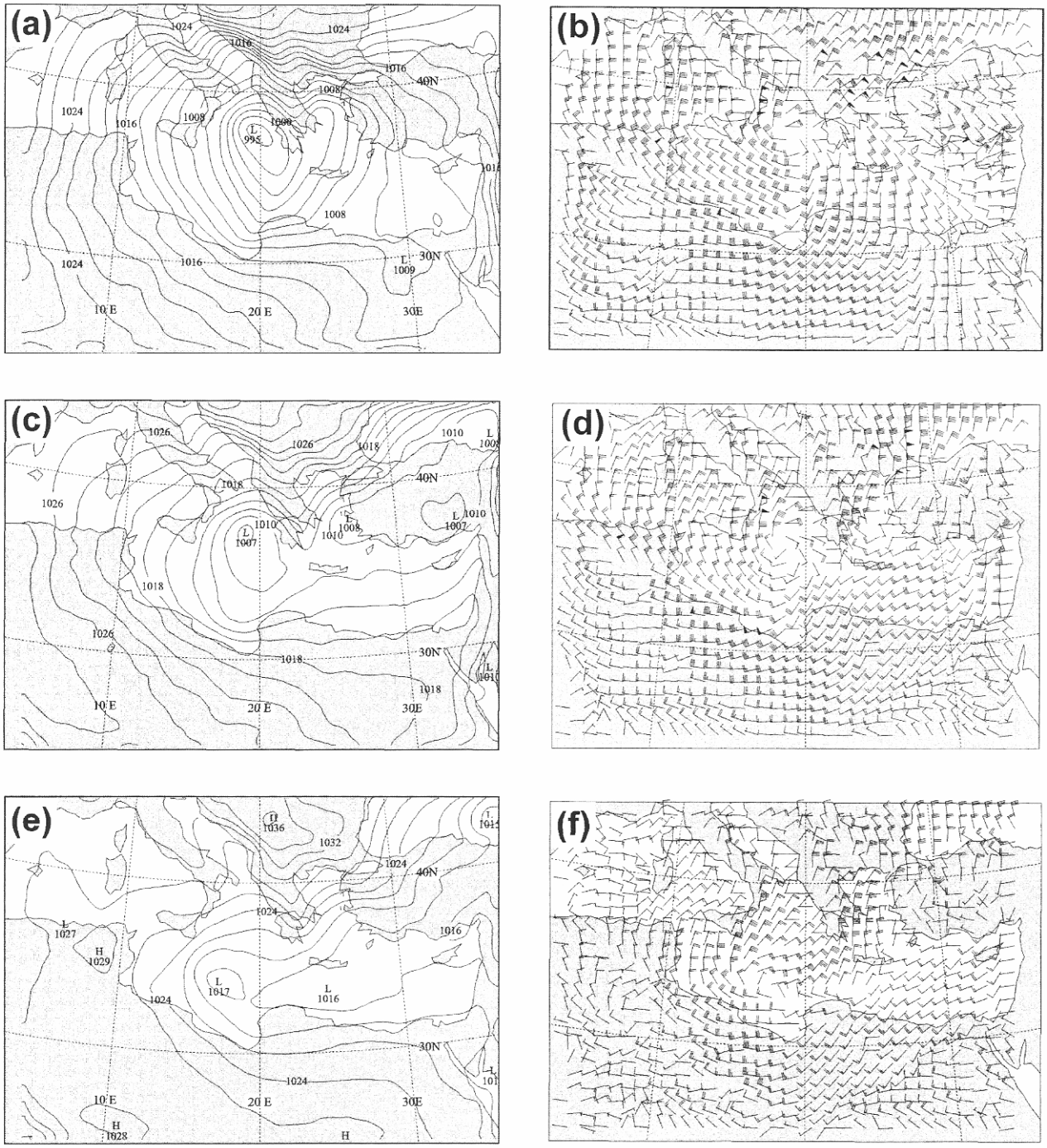

Figure 6. *Eta forecasts of* (a) *sea-level pressure (isobars plotted every 2 hPa and* (b) *lowest model level wind field at 1200 UTC on 14 January (12-hour forecast). One pennant equals 20 m s^{-1}, one barb 4 m s^{-1} and one half-barb 2 m s^{-1}; wind symbols are plotted every fourth grid point.* (c), (d) *As* (a), (b), *but at 1200 UTC on 15 January 1995 (36-hour forecast).* (e), (f) *As* (a), (b), *but at 0600 UTC on 16 January 1995 (54-hour forecast).*

noted that the observed strong flow is better predicted by RAMS than the Eta model. Although RAMS predicted well the southward propagation and the position of the vortex centre during the first 48 hours of model integration, later the predicted vortex seems to accelerate and at 0600 UTC on 16 January it is positioned 100 km farther south than its observed position. The vortex track is summarised later in the text (section 7).

The equivalent potential temperature and absolute vorticity fields at a height of 1050 m AGL at 1200 UTC on 14 January show that the vortex is initially generated within a baroclinic zone. For the θ_e field (Figure 10(*a*)) important horizontal gradients are evident south of Italy; this strong baroclinic zone characterises the area where the vortex has developed. A second baroclinic zone is also observed south of Greece, associated with the cold front which at that time progresses towards

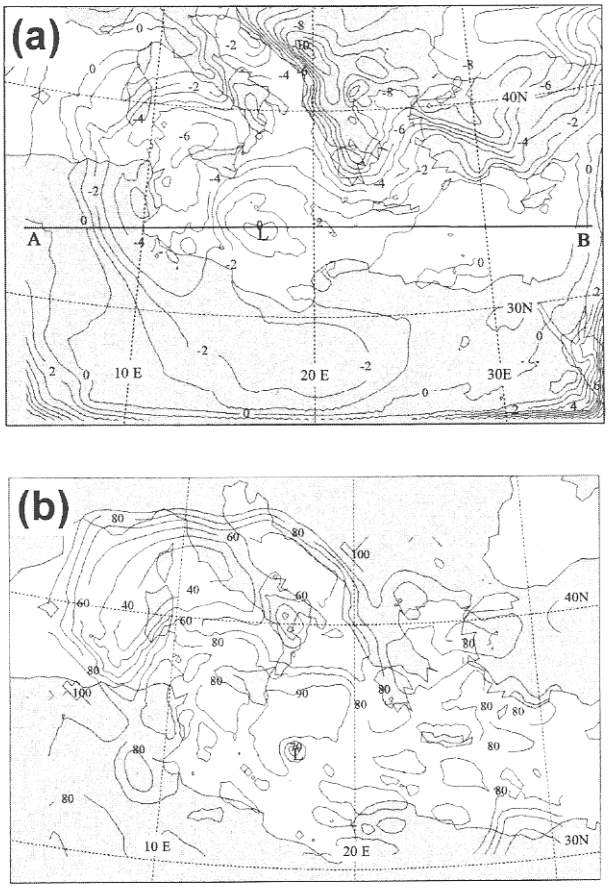

Figure 7. *56-hour Eta forecasts of* (a) *850-hPa temperature (contours plotted every 1 °C) and* (b) *relative humidity (contours plotted every 10%) at 0600 UTC on 16 January 1995 (54-hour forecast). The line* AB *in (a) denotes the cross-section shown in Figure 8. The letter* L *denotes the low centre.*

the east. The same characteristics are also evident in the absolute vorticity field (Figure 10(*b*)), where the area of the parent low was characterised by high absolute vorticity values. Similar structure of the absolute vorticity has also been reported by Rasmussen *et al.* (1996) for a Labrador Sea polar low. During the mature stage of the vortex, the θ_e and the absolute vorticity fields present a symmetric structure around the vortex centre (not shown).

The relatively fine resolution of RAMS Grid 3 (5 km) as well as the explicit microphysical package implemented in the model allow the assessment of the distribution of condensates within the cyclone. Figure 11 shows the mixing ratio of all condensates at 1050 m AGL, at 0600 UTC on 16 January (54-hour forecast), superimposed on the wind field at the same level. The vortex centre is defined by a very weak cyclonic circulation. The condensate mixing ratio on the inner grid depicts a broad band of condensate on the northern and western flanks of the vortex and an area near the centre of the vortex and to its southern flank which is condensate free, while some individual cells are evident on its southern side. The distribution of condensates presented in Figure 11 looks quite similar to the distribution of the higher clouds depicted in the satellite imagery in Figure 2(*c*) (where a cloud-free area characterises the southern flank of the vortex).

An interesting overview of the vortex is presented in Figure 12, where the three-dimensional structure of the equivalent potential temperature is shown at 1200 UTC on 16 January 1996. At this time the 304 K θ_e isosurface has formed a structure like a vertical conduit from the mid-tropospheric layers within the vortex center. This finding is in good agreement with the vertical cross-

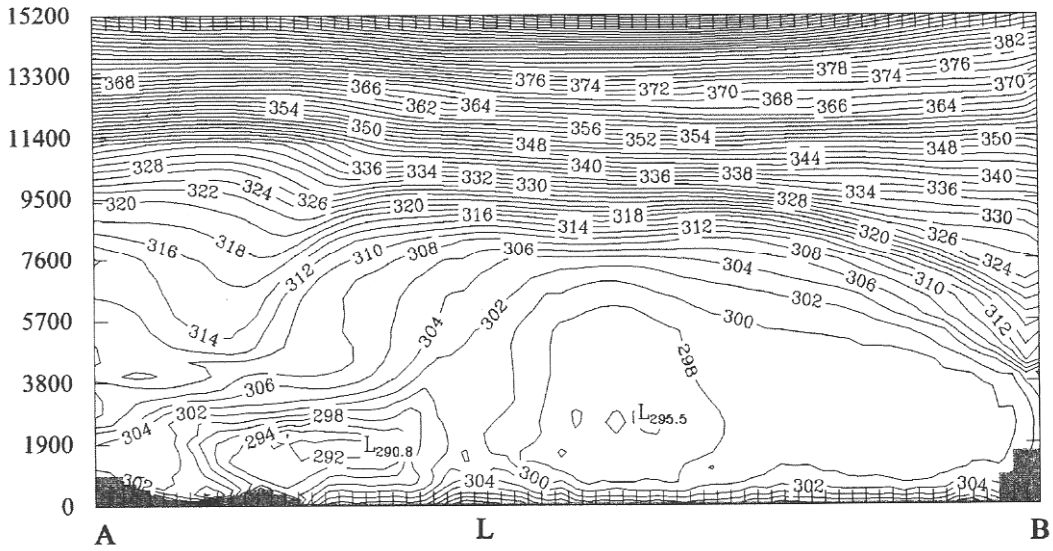

Figure 8. *Vertical cross-sections of the 56-hour Eta forecast of equivalent potential temperature (contours plotted every 2 K) at 0600 UTC on 16 January 1995 (54-hour forecast) following the line* AB *shown in Figure 7*(a). *The letter* L *denotes the position of the vortex centre.*

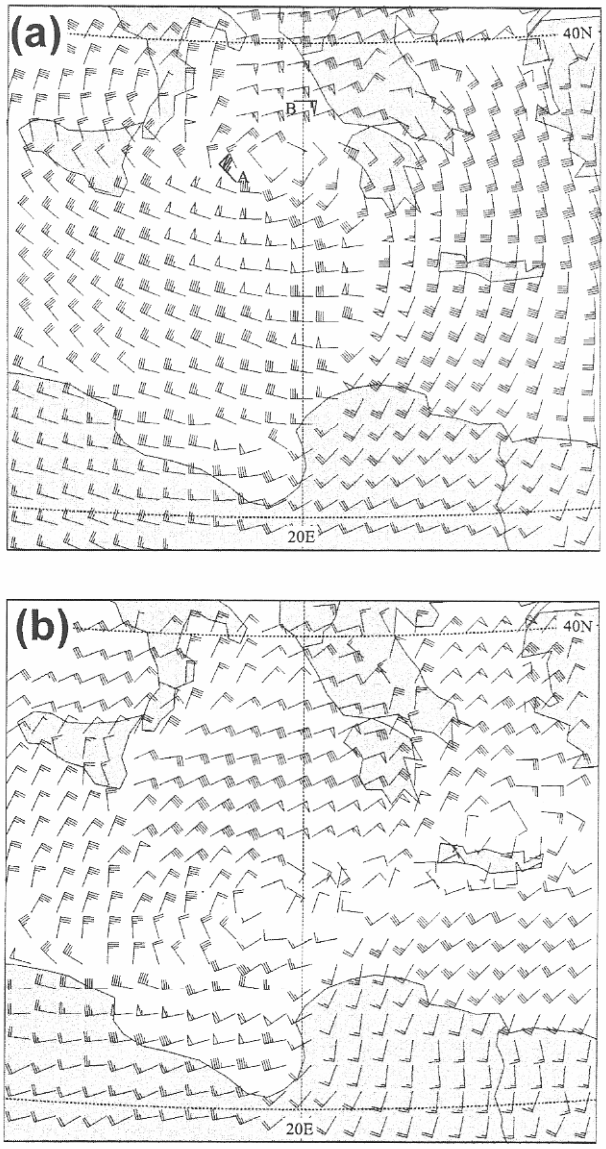

Figure 9. *Wind field forecasts for RAMS Grid 2 at* (a) *1200 UTC on 14 January 1995 (12-hour forecast) and* (b) *0600 UTC on 16 January 1995 (54-hour forecast). Wind symbols are plotted every fourth grid point. One pennant equals 20 m* s^{-1}*, one barb 4 m* s^{-1} *and one half-barb 2 m* s^{-1}*. In* (a) *the letters* A *and* B *and the associated wind barbs in bold correspond to the ship reports given in Figure 3*(a).

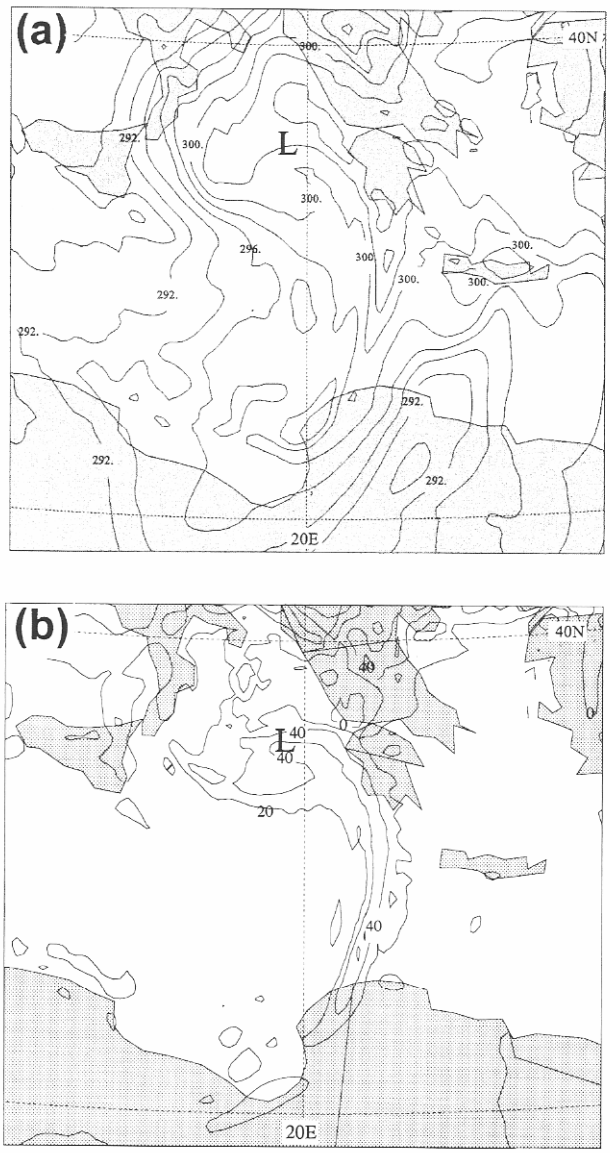

Figure 10. *RAMS forecasts of* (a) *equivalent potential temperature (contours plotted every 2 K) and* (b) *absolute vorticity field (contours plotted every 20 × 10*$^{-5}$ s^{-1}*), at z = 1050 m AGL at 1200 UTC on 14 January 1995 (12-hour forecast). Letter* L *denotes the low centre.*

section inside the Eta domain shown in Figure 8. This three-dimensional structure of θ_e shows also good agreement with that found in the simulated tropical cyclone presented by Tripoli (1992).

6. The role of surface fluxes and latent heat release

Many authors have argued in the past that anomalous sea-surface fluxes of sensible and latent heat may play an important role in the development of vortex-like disturbances over relatively warm water. This idea was first developed for the tropical cyclones (Emanuel, 1986) and then studied thoroughly for polar lows over the Arctic Ocean (e.g. Shapiro *et al.*, 1987; Businger & Baik, 1991) and over the Labrador Sea (Rasmussen *et al.*, 1996) and is referred to as air–sea interaction instability. In order to investigate the role of surface fluxes, predicted sensible and latent heat fluxes from RAMS at 1200 UTC on 14 January (12-hour forecast) are presented in Figure 13. Three regions with sensible heat flux exceeding 200 W m^{-2} are depicted around the region of the parent low, while at the centre of the low sensible heat flux is less than 50 W m^{-2}, corresponding to a higher air temperature and light winds over the low centre (Figure 13(*a*)). This finding is consistent with estimations of sensible heat fluxes reported by Businger

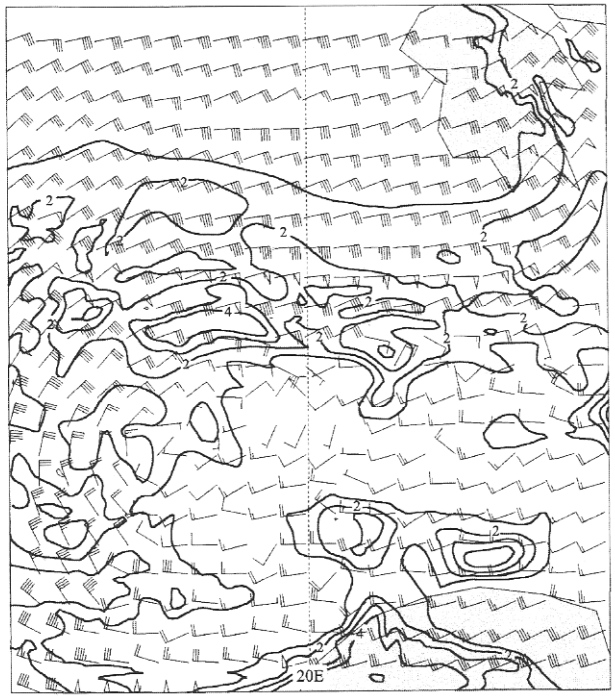

Figure 11. *Condensate mixing ratio (contours every 1 g/kg) and wind field at 1050 m AGL at 0600 UTC on 16 January 1995 (54-hour forecast) inside the inner grid of RAMS. Wind symbols are plotted every fifth grid point. One pennant equals 20 m s^{-1}, one barb 4 m s^{-1} and one half-barb 2 m s^{-1}.*

& Baik (1991) for an Arctic hurricane and by Rasmussen *et al.* (1996) for a Labrador Sea polar low. Latent heat fluxes are more important than sensible heat fluxes, with values exceeding 400 W m^{-2} to the north of the low centre and 500 W m^{-2} on its south-west flanks (Figure 13(*b*)). This structure, with higher values of both sensible and latent heat fluxes around the low centre than at the centre itself, is consistent with previous observations (Businger & Walter, 1988). During the mature stage of the vortex, at 0600 UTC on 16 January, sensible and latent heat fluxes present lower values than during the generation stage of the vortex (not shown). The area around the vortex centre is characterised by heat fluxes lower than 100 W m^{-2}, while higher values are found north of the vortex where strong winds prevail and near the African coast where sea-surface temperature is high and winds exceed 20 m s^{-1}. Alpert *et al.* (1995) have also studied the role of sea fluxes in eastern Mediterranean cyclogenesis and pointed out that generation of secondary cyclogenesis is mainly due to the effect of surface fluxes above the warm Mediterranean waters.

In order to explore the role that the latent heat release within the ascending motions plays on the vortex life-cycle, an additional simulation has been performed where the microphysics parameterisation was switched off. Under this configuration all water in the atmosphere is assumed to occur as vapour and thus there is no latent heat release. The results of this simulation showed that the vortex formed behind the parent low. Later on, when the feeding with cold air was interrupted, the vortex lost its intensity, the winds weakened, and then from the afternoon of 15 January the system began to dissipate (not shown). This result implies that during the mature phase of the vortex, the latent heat release within the updrafts seems to play an important role in maintaining the system.

7. Track of the vortex

Figure 14 gives the vortex tracks at six-hour intervals (starting at 0000 UTC, 15 January 1995) forecast by both numerical models compared to the observed track. The 'observed' centre of the vortex has been sub-

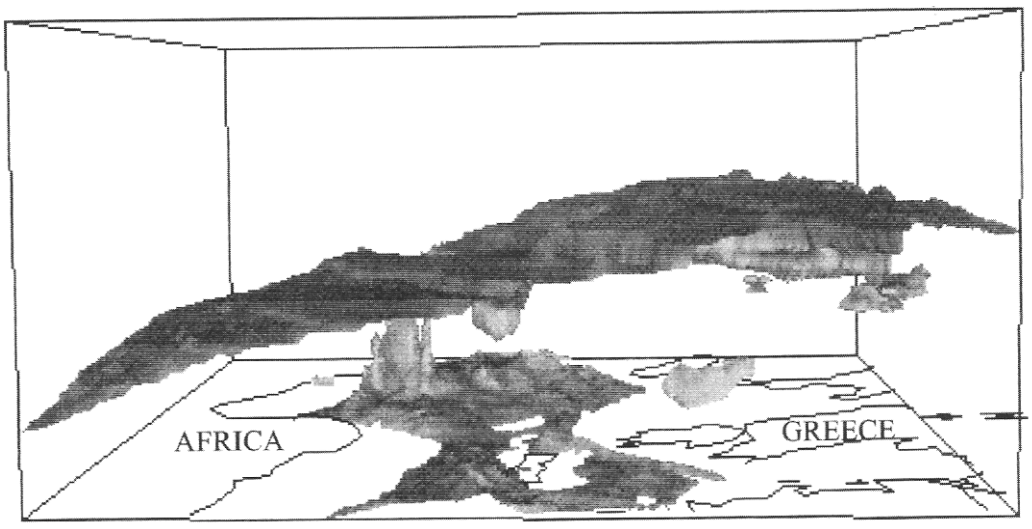

Figure 12. *Three-dimensional structure of the vortex at 1200 UTC on 16 January 1995 (60-hour forecast). Oblique view from the east of the 304 K equivalent potential temperature isosurface using Grid 2 of RAMS.*

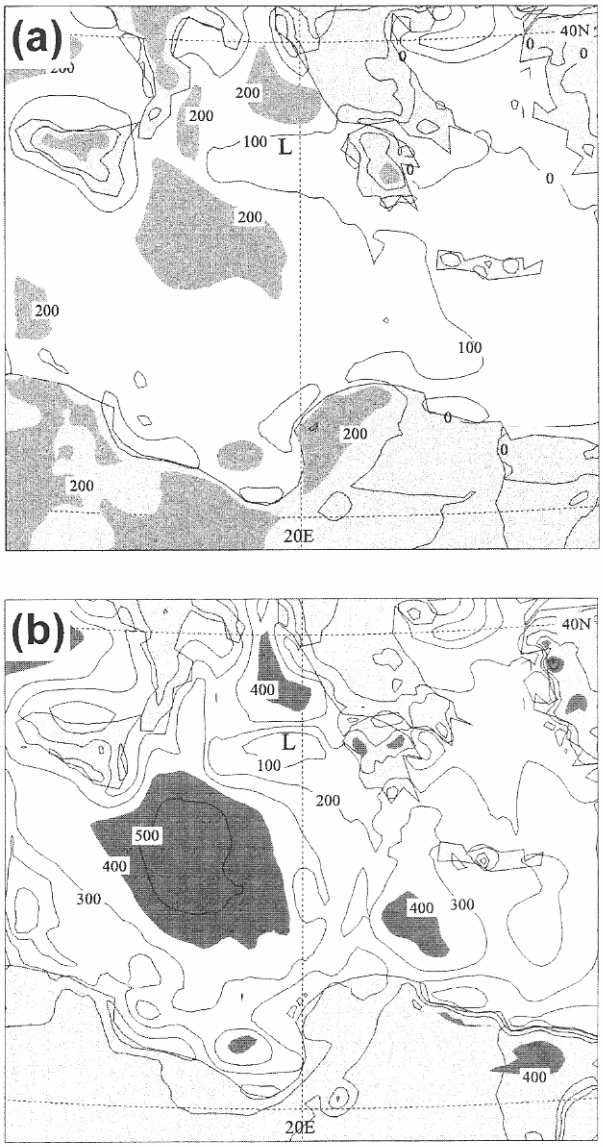

Figure 13. (a) *Sensible heat fluxes (contours plotted every 100 W m^{-2}) inside the second grid of RAMS (areas exceeding 200 W m^{-2} are shaded) and* (b) *latent heat fluxes (areas exceeding 400 W m^{-2} are shaded) for 1200 UTC 14 January 1995 (12-hour forecast).*

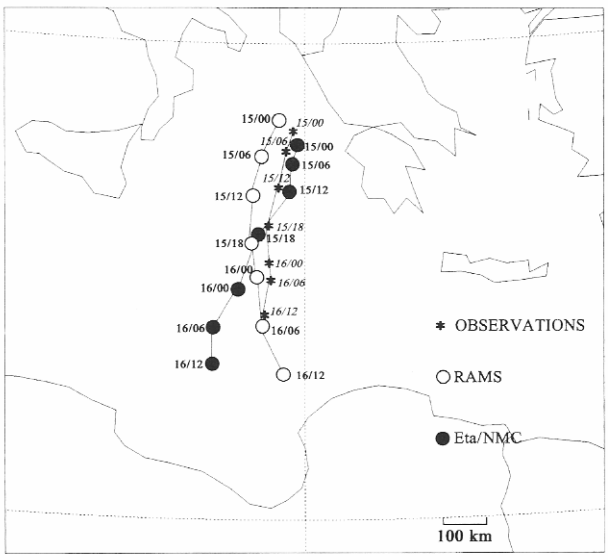

Figure 14. *Successive positions (from north to south) of the observed and forecasted vortex centre from 0000 UTC on 15 January to 1200 UTC on 16 January (60-hour forecast), at six-hour intervals (date/hour). The time of the observed position of the vortex centre is given in italics.*

jectively defined from both the satellite imagery and the sea-level pressure analysis, while the 'forecast' centre has been defined as the location of the minimum sea-level pressure predicted by each model. Note that both models predict quite well the position of the vortex until 0000 UTC on 16 January 1995. The distance between the real and forecast position is not at any instant greater than 50 km. At 0600 UTC on 16 January, both models have predicted a faster propagation of the vortex towards the south, and at 1200 UTC on 16 January the distance between the observed and forecast vortex centre is greater than 150 km. From that time on, the Eta model moved the vortex southwards and dissipated it at the Libyan coasts, in conformity with observations. On the other hand, RAMS failed to accurately forecast this final part of the vortex path, moving the vortex eastwards, where it reached the coast and dissipated.

8. Discussion and conclusions

In the frame of this study the appearance of a Mediterranean vortex has been documented through observational and model analysis. Satellite imagery revealed the existence of a mature vortex, which developed over the sea between Italy and Greece and then followed a path towards the south. The imagery revealed spirally distributed cloud bands around the vortex, a feature which lasted during its whole lifetime. Ship observations evidenced strong winds, well exceeding tropical storm intensity, while they also revealed a warm air mass coinciding with the vortex low centre. These observations compare well with previous observational studies of vortices in the Mediterranean, as well as with polar lows observed in the Arctic.

Although the vortex was associated with an earlier synoptic-scale low, the ECMWF forecasts were not able to track the vortex successfully. This fact prompted the study of this vortex based on simulations performed using two models:

(a) The Eta model, which is currently used for operational forecasts at the Hellenic National Meteorological Service. The successful application of this model for such an event would be very promising as this would provide important guid-

ance for the local forecaster in similar synoptic situations.

(b) The RAMS model, which is an important research tool and could give detailed information on the dynamic and thermodynamic structure of the vortex.

The simulations showed promising results for the prediction of the genesis and life-cycle of this vortex. More precisely, the Eta model correctly predicted the minimum sea-level pressure and the path of the vortex, simulating cyclonic flow structure over the period of more than three days. However, the Eta model failed to reproduce the pressure and wind intensity at the centre of the vortex during the third day of the simulation. On the other hand, the RAMS-predicted wind field was in good agreement with the wind observations from the ships, and thus it succeeded in reproducing the strong winds associated with the vortex. Further, RAMS was able, owing to the detailed microphysics package and the relatively fine resolution of the third grid, to reproduce the cloud structure associated with the vortex.

As pointed out by Emanuel & Rotunno (1989), the air–sea interaction instability requires a pre-existing disturbance to act as a triggering mechanism before the air–sea interaction instability can operate. In this case the vortex developed in a region of low-level baroclinicity associated with a parent low system, while at the 500 hPa level the area west of the surface low was dominated by a cut-off low with temperature <–35 °C. The synergy of the low and mid-tropospheric features acted as the triggering mechanism for the vortex genesis. It is also likely that sensible and latent heat fluxes (with total heat fluxes exceeding 700 W m^{-2}) played a significant role in the deepening of the parent low (from 995 hPa at 0000 UTC on 14 January to 992 hPa at 1200 UTC on 14 January) and the generation of the vortex. Then the vortex became independent of the parent low and it began moving southwards and the feeding with cold air was interrupted; thus during the mature stage of the vortex, surface fluxes were not so important (supported by RAMS calculations of surface fluxes discussed in section 6). During its mature stage the vortex was mainly sustained by latent heat release within the convective motions, as this was implied by the sensitivity simulations performed with RAMS. Then the vortex dissipated when it reached the north African coast.

Following the polar low classification proposed by Businger & Reed (1989) this vortex is characterised as a 'cold-low type', but it should be noted that the low-level baroclinicity and upper-level cold vortex seem to be crucial as a triggering mechanism for the formation of at least this particular Mediterranean vortex.

This study provided some insight into this rare phenomenon of Mediterranean vortices, based on the sparse observations and model results of one case study. A more complete set of observations (including dense upper-air data) would be necessary in order to support the findings of this analysis.

Acknowledgements

The authors are grateful to Ms V. Fragouli (Hellenic National Meteorological Service) for drawing our attention to the appearance of the vortex studied in this paper and to Mr D. Ziakopoulos (Hellenic National Meteorological Service) for his helpful suggestions on the synoptic description of the cyclone. Special thanks are also due to the editor, R.W. Riddaway, for his suggestions, which led to an improvement in the English and grammar of the text. Mr Dominique Dagorne (ORSTOM, Lannion, France) and Mr Stefan Ewald (Institute of Meteorology, University of Hamburg, Germany) are also kindly acknowledged for providing the SSM/I data and algorithms used in this study. The Hellenic National Meteorological Service, and especially Mr G. Potiriadis, is kindly acknowledged for providing the METEOSAT data used in this study. Acknowledgement is also made to the National Center for Atmospheric Research, which is sponsored by the National Science Foundation (USA), for some of the computing time used in this research and for providing the surface data from the operational network used in this study (Contract #35081178).

References

Alpert, P. & Neeman, B. U. (1992). Cold small-scale cyclones over the Eastern Mediterranean. *Tellus*, **44A:** 173–179.

Alpert, P., Stein, U. & Tsidulko, M. (1995). Role of sea fluxes and topography in eastern Mediterranean cyclogenesis. *Global Atmosphere and Ocean System*, **3:** 55–79.

Avissar, R. & Mahrer, Y. (1988). Mapping frost sensitive areas with a three dimensional local scale numerical model. Part I: Physical and numerical aspects. *J. Appl. Meteorol.*, **27:** 400–413.

Betts, A. K. & Miller, M. J. (1986). A new convective adjustment scheme. Part II: Single column tests using GATE wave, BOMEX, ATEX and Arctic air mass data sets. *Q. J. R. Meteorol. Soc.*, **112:** 693–709.

Betts, A. K. (1986). A new convective adjustment scheme. Part E. Observational and theoretical basis. *Q. J. R. Meteorol. Soc.*, **112:** 677–691.

Businger, S. (1985). The synoptic climatology of polar lows outbreak. *Tellus,* **37A:** 419–432.

Businger, S. & Baik J-J. (1991). An Arctic hurricane over the Bering Sea. *Mon. Wea. Rev.*, **119:** 2293–2322.

Businger, S. & Reed, R. J. (1989). Cyclogenesis in cold air masses. *Wea. Forecasting*, **4:** 133–156.

Businger, S. & Walter, B. (1988). Comma cloud development and associated rapid cyclogenesis over the Gulf of Alaska: a case study using aircraft and operational data. *Mon. Wea. Rev.*, **116:** 1103–1123.

Chen, C. & Cotton, W. R. (1987). The physics of the marine stratocumulus-capped mixed layer. *Bound.-Layer Meteorol.*, **25:** 289–321.

Clark, T. L. & Farley, R. D. (1984). Severe downslope windstorm calculations in two and three spatial dimensions

using anelastic interactive grid nesting: a possible mechanism for gustiness. *J. Atmos. Sci.*, **41:** 329–350.

Cotton, W. B., Thompson, T. & Mielke, P. W. (1994). Real time mesoscale prediction on workstations. *Bull. Am. Meteorol. Soc.*, **75:** 349–362.

Cram, J. M, Pielke, R. A. & Cotton, W. R. (1992). Numerical simulation and analysis of a prefrontal squall line. Part II: Propagation of the squall line as an internal gravity wave. *J. Atmos. Sci.*, **49:** 209–225.

Davies, H. C. (1976). A lateral boundary formulation for multi-level prediction models. *Q. J. R. Meteorol. Soc.*, **102:** 405–418.

Douglas, M. W., Fedor, L. S. & Shapiro, M. A. (1991). Polar low structure over the Northern Gulf of Alaska based on research aircraft observations. *Mon. Wea. Rev.*, **119:** 32–54.

Douglas, M. W., Shapiro, M. A., Fedor, L. S. & Saukkonen, L. (1995). Research aircraft observations of a polar low at the East Greenland ice edge. *Mon. Wea. Rev.*, **123:** 5–15.

Emanuel, K. (1986). An air–sea interaction theory for tropical cyclones. Part I: Steady-state maintenance. *J. Atmos. Sci.*, **43:** 584–604.

Emanuel, K. & Rotunno, R. (1989). Polar lows as arctic hurricanes. *Tellus*, **41A:** 1–17.

Ernst, J. A & Matson, M. (1983). A Mediterranean tropical storm? *Weather*, **38:** 332–337.

Janjic, Z.I. (1974) A stable centered difference scheme free of the two-grid-interval noise. *Mon. Wea. Rev.*, **102:** 319–323.

Janjic, Z. I. (1979). Forward–backward scheme modified to prevent two-grid interval noise and its application in sigma coordinate models. *Contrib. Atmos. Phys.*, **52:** 69–84.

Janjic, Z. I. (1984). Non-linear advection schemes and energy cascade on semi-staggered grids. *Mon. Wea. Rev.*, **112:** 1234–1245.

Janjic, Z. I. (1990). The step-mountain coordinate: physical package. *Mon. Wea. Rev.*, **118:** 1429–1443.

Janjic, Z. I. (1994). The step mountain eta coordinate model: further developments of the convection, viscous sublayer, and turbulence closure schemes. *Mon. Wea. Rev.*, **122:** 927–945.

Mayencon, R. (1982). Cyclone en Mediterranee. *Meteorologie Marine*, **117:** 316–319.

McCumber, M. C., & Pielke, R. A. (1981). Simulation of the effects of surface fluxes of heat and moisture in a mesoscale numerical model. Part I: Soil layer. *J. Geophys. Res.*, **86:** 9929–9938.

Mellor, G. L. & Yamada ,T. (1974). A hierarchy of turbulence closure models for planetary boundary layers. *J. Atmos. Sci.*, **31:** 1791–1806.

Mellor, G. L. & Yamada T. (1982). Development of a turbulence closure model for geophysical fluid problems. *Rev. Geophys-Space Phys.*, **20:** 851–875.

Mesinger, F. (1973). A method of construction of second order accuracy difference schemes permitting no false two-grid interval wave in the height field. *Tellus*, **25:** 444–458.

Mesinger, F. (1977). Forward–backward scheme, and its use in a limited area model. *Contrib. Atmos. Phys.*, **50:** 200–210.

Mesinger, F., Janjic, Z., Nickovic, S., Gavrilov, D. & Deaven, D. (1988). The step-mountain coordinate model description and performance for cases of Alpine lee cyclogenesis and for a case of an Appalachian redevelopment. *Mon. Wea. Rev.*, **116:** 1493–1518.

Pielke, R. A, Cotton, W. R., Walko, R. L, Tremback, C. J., Lyons, W. A, Grasso, L. D., Nicholls, M. E., Moran, M. D., Wesley, D. A., Lee, T. J. & Copeland, J. H. (1992). A comprehensive meteorological modelling system – RAMS. *Meteorol. Atmos. Phys.*, **49:** 69–91.

Rasmussen, E. (1981), An investigation of a polar low with a spiral loud structure. *J. Atmos. Sci.*, **38:** 1785–1792.

Rasmussen, E. & Zick, C. (1987). A subsynoptic vortex over the Mediterranean with some resemblance to polar lows. *Tellus*, **39A:** 408–425.

Rasmussen E., Claude, C. & Purdom, J. F. (1996). Labrador Sea polar lows. *Global Atmos. Ocean Systems*, **4:** 275–333.

Santurette, P. (1995). Cyclone ou 'polar low' en Mediterranee. *Meteorologie Marine*, **168:** 23–25.

Schluessel, P. & Luthardt, H. (1991). Surface wind speeds over the North Sea from Special Sensor Microwave/Imager observations. *J. of Geophys. Res.*, **96:** 4845–4853.

Shapiro, M. A, Fedor, L. S. & Hampel, T. (1987). Research aircraft measurements within a polar low over the Norwegian Sea. *Tellus*, **37:** 272–306.

Tremback, C. J. (1990). Numerical simulation of a mesoscale convective complex: model development and numerical results. *Ph.D. dissertation, Atmos. Sci. Paper No. 465*, Colorado State University, Dept. of Atmos. Science, Fort Collins, Co 8523.

Tremback, C. J., Lyons, W. A., Cotton, W. R., Walko, R. L. & Beitler, B. (1994). Operational weather forecasting applications using the Regional Atmospheric Modelling System (RAMS). In *Preprints of the 10th Conference on Numerical Weather Prediction*, Portland, OR, 18–22 July 1994.

Tripoli, G. J (1992). An explicit three-dimensional nonhydrostatic numerical simulation of a tropical cyclone. *Meteorol. Atmos. Phys.*, **49:** 229–253.

Walko, R. L., Cotton, W. R., Meyers, M. P. & Harrington, J. Y. (1995). New RAMS cloud microphysics parameterization. Part I: The single moment scheme. *Atmos. Res.*, **38:** 29–62.

Ziakopoulos, D. & Marinaki, A. (1996). Mediterranean mesoscale vortices with tropical cyclone features. In *Proc. of the 3rd Hellenic Conference on Meteorology, Climatology and Physics of the Atmosphere*, 25–27 September, Athens, Greece, 154–159.